Engagement-Free and Contactless Bed Occupancy and Vital Signs Monitoring

Yingjian Song, Bingnan Li, Dan Luo, Zaipeng Xie, Bradley G. Phillips, Yuan Ke, and Wenzhan Song, *Senior Member, IEEE*

***Abstract*—This article presents the design and evaluation of an engagement-free and contactless vital signs and occupancy monitoring system called BedDot. While many existing works demonstrated contactless vital signs estimation, they do not address the practical challenge of environment noises, online bed occupancy detection, and data quality assessment in the real-world environment. This work presents a robust signal quality assessment algorithm consisting of three parts: 1) bed occupancy detection; 2) movement detection; and 3) heartbeat detection, to identify high-quality data. It also presents a series of innovative vital signs estimation algorithms that leverage the advanced signal processing and Bayesian theorem for contactless heart rate (HR), respiratory rate (RR), and interbeat interval (IBI) estimation. The experimental results demonstrate that BedDot achieves over 99% accuracy for bed occupancy detection, and MAE of 1.38 BPM, 1.54 BPM, and 24.84 ms for HR, RR, and IBI estimation, respectively, compared with an FDA-approved device. The BedDot system has been extensively tested with data collected from 75 subjects for more than 80 h under different conditions, demonstrating its generalizability across different people and environments.**

***Index Terms*—Bed occupancy, Contactless Monitoring, heart rate (HR), interbeat interval (IBI), respiratory rate (RR), sleep, vital Signs.**

I. Introduction

THE CONTINUOUS monitoring of vital signs, such as heart rate (HR), respiratory rate (RR), and interbeat interval (IBI) during sleep, has numerous critical applications. For example, monitoring HR can aid in predicting—and even preventing—heart failure while asleep. Sleep apnea can be detected by monitoring RR [1]. Additionally, IBI has been used for heart rate variability (HRV) analysis. This analysis contributes not only to the understanding of atrial fibrillation [2] but also to stress analysis [3], [4].

In the literature, various approaches for sleep activity and health monitoring have been explored. These can be categorized into the following.

1) *Wearables* [1], [5], [6], [7], [8], [9] are perhaps the most popular human activity monitoring device today because they can accompany a person anywhere and anytime. However, they may not be suitable for everyone. Their need for skin contact can make some users uncomfortable during sleep. Additionally, elderly users often forget to recharge their batteries, and maintaining patient engagement poses a significant challenge. According to the Center for Medicare and Medicaid Services (CMS), the compliance rate for patients provided with wearable devices to monitor their own vital signs is disappointingly low (around 5%), which puts remote patient monitoring programs at risk. Moreover, these devices typically lack bed occupancy detection features, such as detecting when a person gets on or off the bed.
2) *Sleep pads* (based on MEMS, FPG, and pressure sensor based) [10], [11], [12], [13] are generally positioned between the mattress and the box spring, or between the bed-sheet and the mattress. These devices predominantly rely on pressure sensors and require the user's heart to be positioned vertically above the pad to accurately capture vital signs. However, disturbances, such as movements of the bed sheet, wetness due to enuresis, or changes in sleeping position can impair the functionality of these pads.
3) *Bedside monitors*, which include radar [14], [15], [16] and camera systems [17], [18], [19], [20], are either installed above the bed or positioned on the bedside table. Radars work by emitting probing waves toward the heart and utilizing the reflected waves to calculate vital signs and analyze sleep quality. Continuous operation implies continuous radiation exposure, a health concern for some. Camera-based solutions, even those using thermal cameras that produce obscured recordings [19], often raise privacy concerns, especially given their installation in bedrooms. Setting up these technologies often demands meticulous adjustments to angles and distances to effectively capture the subjects' facial areas. A more detailed survey of these approaches is provided in Section II.

Manuscript received 14 August 2023; revised 3 September 2023; accepted 14 September 2023. Date of publication 18 September 2023; date of current version 21 February 2024. This work was supported by NIH under Grant UL1TR002378. The work of Bradley G. Phillips was supported in part by the Georgia CTSA under Grant UL1TR002378. The work of Yuan Ke was supported in part by NSF-DMS under Grant 2210468. The work of Wenzhan Song was supported in part by NSF-STTR under Grant 1940864, and in part by the Georgia Research Alliance under Grant DOE-EE0009026, Grant NSF-SaTC-2019311, and Grant DOD-FA8571-21-C-0020. *(Corresponding author: Wenzhan Song.)*

This work involved human subjects or animals in its research. Approval of all ethical and experimental procedures and protocols was granted by IRB under Application No. PROJECT00001838.

Yingjian Song and Wenzhan Song are with the School of Electrical and Computer Engineering, University of Georgia, Athens, GA 30602 USA (e-mail: yingjian.song@uga.edu; wsong@uga.edu).

Bingnan Li, Dan Luo, and Yuan Ke are with the Department of Statistics, University of Georgia, Athens, GA 30602 USA (e-mail: bingnan.li1@uga.edu; dl43052@uga.edu; yuan.ke@uga.edu).

Zaipeng Xie is with the College of Computer and Information, Hohai University, Nanjing 210098, China (e-mail: zaipengxie@hhu.edu.cn).

Bradley G. Phillips is with the Clinical and Translational Research Unit, University of Georgia, Athens, GA 30602 USA (e-mail: bgp@uga.edu).

Digital Object Identifier 10.1109/JIOT.2023.3316674

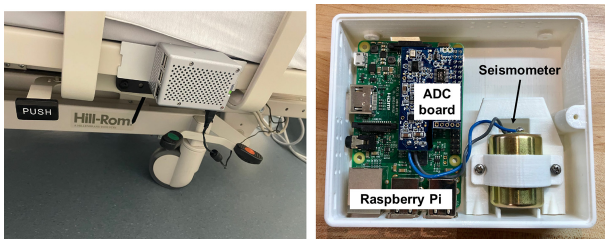

Fig. 1. Installation of BedDot on the side of bed frame (right), BedDot device (left).

In this article, we introduce BedDot, a novel sleep and vital signs monitoring system based on passive seismic sensing. This system addresses many of the previously mentioned limitations. Notably, it alleviates privacy concerns by avoiding the capture of images or voices, does not require direct contact with the human body, and eliminates the need for active patient engagement. We have successfully deployed BedDot for real-time monitoring of sleep and vital signs in both home and hospital settings. The design and components of BedDot are illustrated in Fig. 1. The system consists of a Raspberry Pi that acts as the onboard computer, an analog–digital converter (ADC) board, and a vertical geophone that functions as a vibration detector (seismometer). The geophone contains a magnetic element encircled by wire coils. As the magnetic element moves within these coils, an electrical signal is produced. This geophone sensor can capture micro-vibrations produced by human cardiac activity in real time, showcasing a sensitivity level that significantly surpasses most MEMS accelerometers [21]. The ADC board digitizes the data at a sampling rate of 100 Hz. This high sensitivity allows BedDot to measure cardiac activity without physical contact. A comparison between BedDot and other existing sensors will be explored in Section II. Through our research, we have found that the BedDot system attains over 99% accuracy in bed occupancy detection. It also has an mean absolute error (MAE) of 1.38 BPM for HR, 1.54 BPM for RR, and 24.81 ms for IBI estimation when compared with an FDA-approved device. We extensively tested our system using data collected from 75 subjects over more than 80 h in varied conditions, further demonstrate its versatility and adaptability across diverse individuals and environments.

To achieve our results, several *significant technical challenges* were addressed, as detailed below.

1) *Bed Occupancy Detection:* Most existing work in bed occupancy detection focuses on identifying the "moment of bed entry" and the "moment of bed exit." However, simply detecting bed entry and exit can lead to substantial errors if false detection occurs even once. First, the outputs of the geophone are not always zero due to environmental noise, even when there is no person in the bed. Therefore, merely checking signal amplitude to detect bed occupancy will fail. Although the signal energy of bed entries and exits is typically much higher than other types of signals, significant movements on the bed can lead to false detection and subsequent cascade failures. Second, even when there is no person on the bed, vibrations from events around the bed, such as footsteps or other periodic vibrations, can mimic the waveform properties of a heartbeat, leading to false detection.
2) *HR Estimation:* The waveform of the collected heartbeat signal in our system varies depending on factors, such as sensor location, types of beds, environmental noise, and individual differences among people. These variations create difficulties in accurately estimating HR. Moreover, some heartbeat signals show both systolic and diastolic peaks within one cardiac cycle, leading to an estimation that could be twice the actual rate if standard peak detection algorithms are applied.
3) *RR Estimation:* Geophone-based RR estimation poses challenges because the frequency of respiration signals is low and easily influenced by environmental noise. Previous geophone-based work for RR estimation has relied on a square-law amplitude demodulation algorithm [21], which assumes that respiration causes amplitude fluctuations in the geophone signal. However, this approach does not adequately reveal the respiration pattern from the geophone signal. Although high-quality data can clarify heartbeat patterns, detecting respiration patterns is problematic with geophones. They are often insensitive to low-frequency vibrations, which makes estimating the RR difficult. The slow vibration speed caused by respiration is frequently obscured by noise and heartbeat patterns.
4) *IBI Estimation:* Often, the heartbeat peak within each cardiac cycle is obscured by noise, making it more challenging to accurately locate the heartbeat peak position for IBI estimation. As a result, conducting heartbeat peak detection on raw or even denoised data leads to suboptimal performance.

The *major contributions* of this article are summarized as follows.

1) We design an automatic signal quality assessment algorithm to detect bed occupancy, select high-quality data, and prevent undesirable outcomes in subsequent HR, RR, and IBI estimation. The system autonomously identifies when a person is on the bed and initiates calculations for HR, RR, and IBI once the signal quality meets the required threshold.
2) We develop novel signal processing algorithms to denoise signals and extract salient features for HR, RR, and IBI estimation. These algorithms reconstruct the waveform of heartbeat and respiration signal envelopes. By applying the Bayesian theory, we fuse features to enhance the accuracy of HR and RR estimation. A series of mathematical formulations underpin the approach, which has demonstrated strong performance in real-world deployments. We rigorously test the algorithm on 75 subjects across varied conditions, highlighting the broad applicability, and robustness of our methods.
3) We showcase the efficacy of the BedDot system in monitoring both beds and seats, achieving excellent performance in HR, RR, and IBI estimation. The accuracy levels for HR and RR conform to FDA standards. To the best of our knowledge, ours is one of the first to employ a geophone-based system that accurately estimates HR, RR, and IBI across both seats and beds.

The remainder of this article is organized as follows. Section II delves into related works, covering both bed occupancy detection and contactless vital sign monitoring. In Section III, we elucidate the methodology of our system, encompassing bed occupancy detection, movement detection, and the estimation of HR, RR, and IBI. Section IV outlines the experimental setup and system visualization, followed by a presentation of the evaluation results. We draw our conclusions in Section V.

II. Related Works

A. Bed Occupancy Detection

Pouliot et al. [22], Taylor et al. [23], and Braun et al. [24] established a baseline threshold when no one is on the bed, utilizing it as prior knowledge. This threshold is subsequently used to compare with incoming signals to ascertain the bed occupancy status. Such methods are straightforward and intuitive. However, these references lack statistical results for this approach, complicating performance evaluation. Moreover, it necessitates reinitialization for different environments. Clemente et al. [25] introduced a feature fusion method that combines Spectral Entropy, Kurtosis, and the Teager Energy Operator to identify bed entries and exits. While they achieved high accuracy with their data set, their approach is limited to detecting moments of "bed entry" and "bed exit" rather than continuously discerning "on bed" or "off bed" status. Such an approach might introduce persistent errors if a single bed entry or bed exit event is inaccurately detected. Li et al. [26] employed an autocorrelation function (ACF) to determine the periodicity of signals, distinguishing between on bed and off bed signals. This technique can achieve impressive accuracy. However, its efficiency diminishes when signals other than heartbeats—yet still periodic—interfere, potentially resulting in false detections.

B. Contactless Vital Sign Estimation

Technologies that rely on cameras [17], [18], [19] often raise privacy concerns, particularly when the subject is in bed. Even thermal cameras, which generate blurred video recordings [19], can be intrusive. Additionally, the setup for camera-based technologies can be complex, necessitating precise adjustments of angles and distances to effectively capture the subject's facial area. A failure to capture complete facial features can significantly reduce the accuracy of vital signs estimation. The installation of fiber bragg grating sensors (FBGs) [27], [28] presents its own set of challenges. These sensors can be complex and cumbersome to install, especially considering variations in bed size and human anatomy. Moreover, the need to position FBGs between the human body and the mattress may lead to discomfort during sleep. Similar issues extend to sleep pads [29], [30], which are typically placed between the mattress and the box spring, or between the bed sheet and the mattress. These pads often use pressure sensors, such as air, PVDF, fiber, and MEMS pressure sensors. However, to capture vital signs accurately, the heart must be vertically aligned above the pad or belt. Factors, such as the movement of bed sheets, wet sheets due to enuresis, or changes in sleep positions frequently cause these sleep pads to malfunction.

Contactless sleep monitoring of vital signs has become a popular research topic in recent years. For example, Yang et al. [20] used two radio devices to receive the signal reflected from the human body and apply a fast Fourier transform (FFT) to transform the signal from the time domain to the frequency domain. They then perform FFT denoising to simulate a bandpass filter in the frequency domain. After that, they apply an inverse FFT to the filtered frequency domain to recover a smoothed signal in the time domain. Finally, they estimate HR and RR by counting peaks in the filtered data. In a similar vein, Rahman et al. [14] used Doppler Radar and microwave signals to detect air vibrations caused by heartbeat and respiration. They apply bandpass filter signals with different frequency range cutoffs and then perform FFT on the filtered signals to estimate HR and RR. While their methods are simple to implement, they may not be applicable to signals with more complex waveforms.

Vogels et al. [31] introduced a sleep monitoring system based on a near-infrared (NIR) camera. They extract pulse signals from continuous NIR frames using the PBV algorithm [32] and then apply FFT to the extracted signal to determine pulse rates. However, their system cannot estimate RR. Moreover, the use of a camera-based system raises potential privacy concerns that need to be considered.

The methodologies presented in [10], [11], [12], and [13] utilize specialized mattresses with integrated sensors to capture ballistocardiography (BCG) and estimate HR and RR. Likewise, [33] employs load cells, while both [34] and [35] utilize Electromechanical film sensors for HR and RR monitoring. While these approaches produce satisfactory estimation results, it is noteworthy that their setup procedures are relatively intricate.

The study in [27] introduced an innovative design for an FBG mattress, incorporating 13 FBG sensors. This method identifies the most informative sensor by selecting the one with the highest peak in the power spectrum for subsequent HR estimation. However, the efficacy of this approach could be significantly compromised if the dominant frequency of the selected sensor lies outside the typical HR range.

Vehkaoja et al. [36] proposed an IBI algorithm based on segment correlation of the signal, which necessitates post-correction. Similarly, [37] introduces a robust IBI estimation algorithm that has been widely referenced in literature and is often set as a baseline method. However, their approach requires segmenting the signal into multiple portions and applying a convolution operation to each segment. This significantly increases the computational cost and may not be suitable for real-time systems.

A previous geophone-based system [38] utilized a geophone to capture vibration signals resulting from heart movements. For HR estimation, they initially applied a low-pass filter to differentiate between noise and heartbeat data. Following this, they employed a peak-finding algorithm [39] on the ACF of the raw signal for HR estimation. In their subsequent research [21], they introduced an RR estimation algorithm rooted in square-law amplitude demodulation. Instead of performing peak detection on denoised data, they focused on the ACF of the denoised data. Utilizing ACF on the raw signal can yield more pronounced heartbeat peaks when compared to both raw and

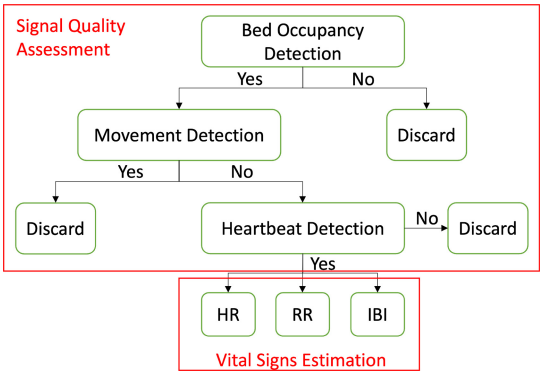

Fig. 2. Work flow of vital signs monitoring by BedDot.

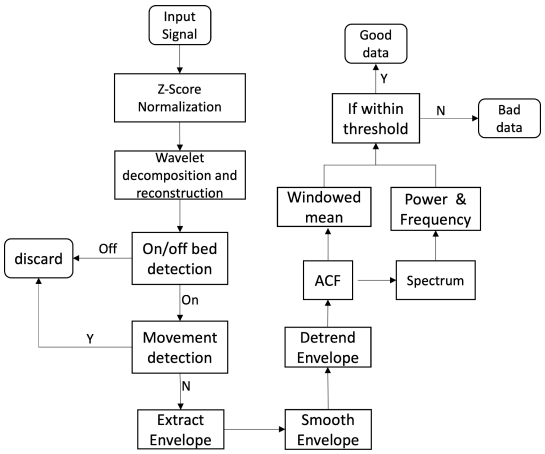

Fig. 3. Signal quality assessment algorithm.

denoised data. However, applying ACF directly to denoised data can produce numerous small peaks, the majority of which are not indicative of heartbeats. This can undermine the effectiveness of the peak detection algorithm, leading to inconsistent results. Furthermore, the peak detection algorithm necessitates a threshold, the optimal selection of which can be challenging due to diverse waveform variations. While they pursued RR analysis through square-law amplitude demodulation, the fundamental approach was to combine a low-pass filter with FFT. This method, albeit straightforward, is not very stable, and its performance leaves room for improvement.

Another geophone-based system, as presented in [25], initially applies a band-pass filter. They subsequently extract the envelope by detecting peaks and connecting them. After extracting the envelope, they identify its local maxima and set a threshold to discard outliers. The final step involves calculating the HR by averaging the intervals between detected peaks. For RR estimation, they create an RR envelope by interpolating the peaks on the HR envelope. Their approach, rooted in the use of the envelope for HR and respiration rate estimation, is both intuitive and straightforward. However, their method of envelope extraction exhibits noticeable boundary issues at both the beginning and end of the signal. Moreover, peak detection on the envelope can be unstable, especially if the envelope is riddled with noise or consists of numerous small spikes that are challenging to remove.

The previously discussed works did not address a system's capacity to automatically procure high-quality data via bed or seat occupancy detection. This aspect is pivotal in circumventing undesired outcomes and ensuring precise vital signs estimation.

III. Methodology

The workflow of the BedDot system is illustrated in Fig. 2. The geophone within BedDot collects raw data, typically positioned beneath the bed frame for monitoring human vital signs. In this section, we discuss the signal quality assessment methods, encompassing bed occupancy detection, movement detection, heartbeat detection, and HR estimation. Subsequently, we delve into the algorithms used for RR and IBI estimation.

A. Signal Quality Assessment and Heart Rate Estimation

For accurate estimation of HR, RR, and IBI using the seismic signal gathered by BedDot, it is crucial to filter out the noise and other vibrations unrelated to vital activities. The signal is a combination of diverse vibration sources: background white noise, household appliance disturbances (e.g., air conditioners, washers, and dryers), bodily movements during sleep, and vital activity vibrations, such as heartbeats, respirations, and blood pressure fluctuations. Our algorithm starts by determining the presence of a person on the bed. If confirmed, the algorithm assesses the signal for any movement that distorted waveform of signals. Only signals showcasing clear and identifiable heartbeats proceed to the vital sign estimation stage. The comprehensive workflow of the signal quality assessment algorithm can be viewed in Fig. 3.

1) Data Preprocessing: The z-score transformation standardizes the signa x as $\widetilde{x} = [x - mean(x)]/std(x)$ where $mean(x)$ and $std(x)$ represent the mean and standard deviation of x, respectively. The signal collected by BedDot originates from body mass movements influenced by cardiac activity. To filter out noise from this signal, we employ discrete wavelet decomposition. We prefer wavelet denoising over bandpass filtering for two main reasons: 1) Wavelet denoising exhibits fewer boundary issues in comparison to a zero-phase-shift bandpass filter and 2) while a bandpass filter blocks all out-of-band noise, it does not specifically denoise within the passband. In contrast, wavelet denoising breaks down a noisy signal into various scales, effectively eliminating noise, and preserving the core signal, irrespective of its frequency range.

For wavelet denoising, the daubechies 12 (db12) is chosen as the mother wavelet due to its resemblance to the cardiac cycle observed in our collected signal. Discrete wavelet decomposition aims to separate the signal into different frequency ranges. During this decomposition, signals undergo both a low-pass filter $y_{\text{low}}[n] = \sum_{k=-\infty}^{\infty} x[k]l[2n-k]$ and a high-pass filter $y_{\text{high}}[n] = \sum_{k=-\infty}^{\infty} x[k]h[2n-k]$.

Here, $l[\cdot]$ represents for low pass filter with y_{low} as the decomposed low-frequency signal. Meanwhile, $h[\cdot]$ is the high-pass filter, with y_{high} being the decomposed high-frequency signal. The variable x denotes the previously decomposed low-frequency signal. With each decomposition, the signal's frequencies are halved. For instance, if the frequency range of x is denoted as $[0, f]$. These frequencies are divided into a low-frequency range $[0, f/2]$ and a high-frequency range

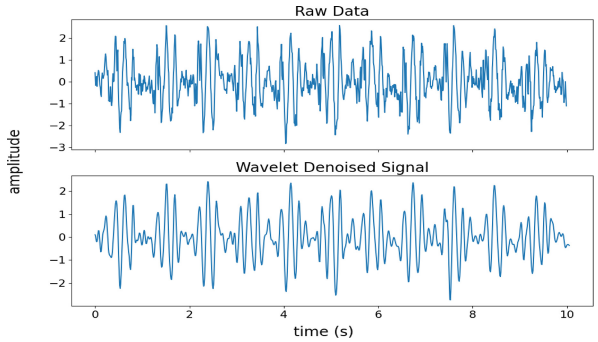

Fig. 4. Top row of the figure shows raw data while the bottom row of the figure shows the wavelet decomposition and reconstructed signal.

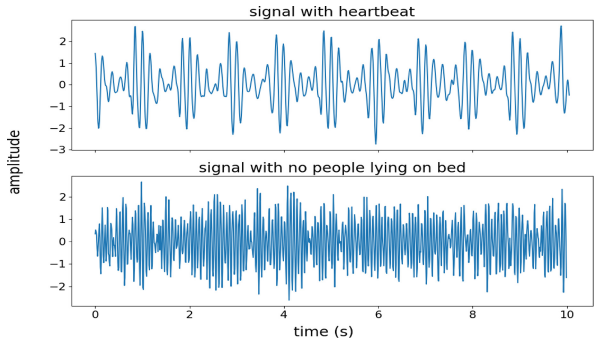

Fig. 5. Figure at the top shows the signal that contains clear heartbeats. The figure at the bottom displays the signal with no person lying on the bed. It can be easily observed that the signal on the bottom fluctuates more.

$[f/2, f]$. The output from the low-pass filter is then subjected to another round of decomposition using a new set of low-pass and high-pass filters.

Given that the sampling rate of our signal is 100 Hz and according to the Nyquist–Shannon sampling theorem that the valid frequency range extends up to 50 Hz. After decomposing the signal six times, we obtain seven distinct components. The frequency ranges for these components, starting from D1 up to D6 and followed by A1, are $[25, 50]$, $[12.5, 25]$, $[6.25, 12.5]$, $[3.125, 6.25]$, $[1.5625, 3.125]$, $[0.78125, 1.5625]$, and $[0, 0.78125]$ Hz, respectively. For this analysis, we opt for the decomposed components with frequency ranges spanning 0.8 to 12 Hz, encompassing D3 to D6, to reconstruct the denoised signal. An illustration of the wavelet denoising process can be found in Fig. 4.

2) Bed Occupancy Detection: After conducting wavelet decomposition and reconstruction on the raw data, we derived a denoised signal. One primary functionality of BedDot is to determine whether the bed is occupied, essentially functioning as an on/off-bed detection algorithm. As highlighted in Section I, bed occupancy detection faces two primary challenges. First, the inherent system errors of the geophone complicate direct person detection on the bed-based solely on amplitude. Relying solely on signal energy to detect bed entry and exit can lead to cascading errors. Second, during the periods designated as on bed and off bed, other vibrations or interference may occur, potentially undermining the accuracy of bed occupancy detection.

To Address the First Challenge, we distinguish the on bed signal from the off bed signal by capitalizing on the waveform distinctions between the two signal types. Drawing inspiration from the speech detection in audio signal processing, we compute the zero crossing rate (ZCR) of the denoised signal. This aids in distinguishing the on bed signal from the off bed signal. The ZCR quantifies the frequency with which a signal shifts from positive to negative and vice versa: $\text{zcr} = (1/N-1)\sum_{i=1}^{N-1} 1_{\mathbb{R}<0}(x_i \cdot xi - 1)$, where zcr represents the ZCR, x denotes a signal of length N, and $1_{\mathbb{R}<0}$ is an indicator function. The ZCR is often employed in audio processing to ascertain the presence of speech within a signal. This is because the amplitude of a signal containing speech typically rises abruptly and oscillates less than the background noise. As a result, the ZCR for speech segments is considerably lower than for audio segments devoid of speech.

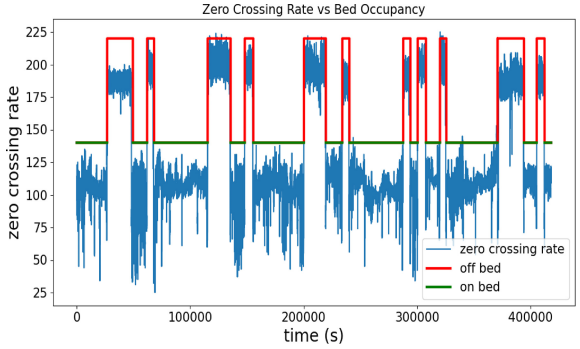

Fig. 6. "Signal with no person lying on bed" (red lines) shows a higher ZCR than "signal with people lying on bed" (green lines).

ZCR serves as an insightful metric for the waveform's shape, providing a measure of the signal's frequency in the time domain. Drawing a parallel with audio signals, the heartbeat when a person is on bed can be likened to "speech," whereas environmental vibrations can be equated to "background noise." It is evident that a signal incorporating the heartbeat exhibits significantly fewer oscillations compared to the signal when no individual is on the bed, as depicted in Fig. 5. Our empirical analysis is consistent with this hypothesis. We observed that the ZCR during an on-bed phase was markedly lower than during an off-bed phase. This observation is vividly illustrated in Fig. 6, which presents the ZCR over a week of sleep monitoring for an individual. The red rectangle in Fig. 6 is the off-bed period, while the green rectangle indicates the on-bed span. Notably, the off-bed period consistently show a higher ZCR.

To Address the Second Challenge, which involves distinguishing vibrations caused by footsteps or other environmental factors from signals containing the heartbeat, we employ the kinetic energy change between two consecutive time steps. This approach is grounded in the understanding that events leading to vibrations, such as footsteps, would abruptly alter the signal's waveform, thereby producing numerous high spikes and resulting in a substantial shift in the signal energy compare to regular background noise signal. In our algorithm, we first calculate the energy of the signal in each time step using the $e(T) = (1/2) \cdot m \cdot \sum_{t=T-N}^{T} v(t)^2$, where $e(T)$ is the kinetic energy for a signal segment of length N, $v(t)$ is the measured velocity in time t, and m is the mass of the object.

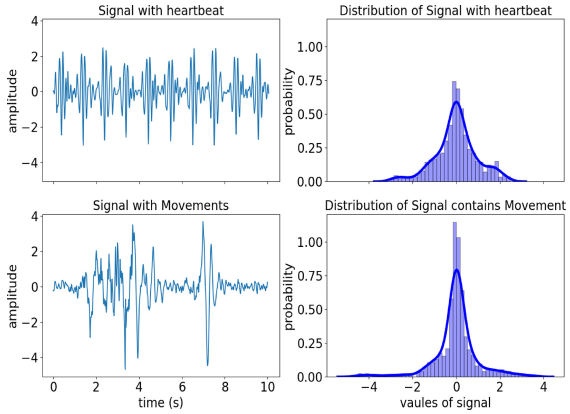

Fig. 7. Distributions for 10-s signals with heartbeats and 10-s signals with movements.

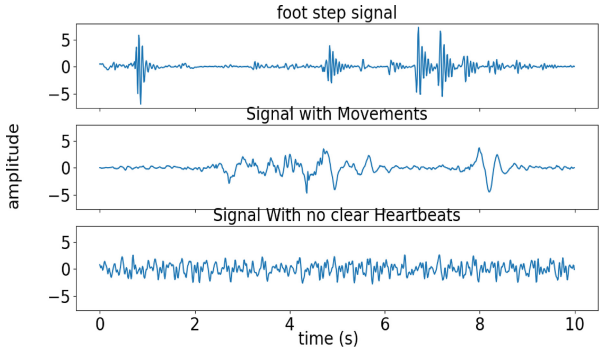

Fig. 8. Signal contains movement(foot step) caused by events around bed (top). Signal with people lying on bed but containing movement (middle). On-bed signal with no clear heartbeat (bottom).

Subsequently, we calculate the difference between the energy of two consecutive time steps as follows:

$$\Delta E_P(T_2) = \frac{|e(T_2) - e(T_1)|}{e(T_1)} = \frac{|\sum_{t=T_2-N}^{T_2} v(t)^2 - \sum_{t=T_1-N}^{T_1} v(t)^2|}{\sum_{t=T_1-N}^{T_1} v(t)^2}. \quad (1)$$

We establish a threshold value on the energy changes for differentiating a person's heartbeat from those caused by footsteps or other environmental vibrations. If $\Delta E_P(T_2)$ exceeds the threshold, we categorize it as an external event. Based on extensive empirical testing with large data sets, we have set the threshold at 20%. In essence, our bed occupancy detection algorithm integrates both the ZCR and energy change metrics to effectively differentiate between signals containing heartbeat patterns and those instigated by external events. Subsequently, the bed occupancy status for "external events" signals will be determined as "uncertain" which is neither on bed or off bed. The final status of external events signals will be decided by bed occupancy status prior to and followed after external events. External events signal status will be the same as both status if the status prior to and followed after external events are the same. Otherwise, the status of external events signal will be the same as bed occupancy status followed after external events.

3) Movement Detection: Once we have successfully determined that the bed is occupied, it is essential to further assess the status of the person on the bed. This is because their movements can introduce distortions on vibration signals collected by BedDot. As depicted at the bottom of Fig. 8, certain portions of the signal are influenced by movements on the bed. Typically, in-bed movements produce pronounced vibrations, resulting in a higher number of outliers in the gathered data. This leads to a significant disparity in the distribution of signals when compared to those unaffected by motion artifacts. This contrast is illustrated by comparing the distributions of movement-affected signals with those of pure heartbeat signals in Fig. 7.

Leveraging our observations, we propose using Kurtosis as a method to detect whether a segment of the signal is affected by movements. Kurtosis quantifies the centered fourth moments of a distribution, and it is frequently employed to detect the presence of outliers or to ascertain if errors have heavy tails. For a random sample $\{x_i\}_{i=1}^n$, the empirical Kurtosis is computed by $\kappa_x = ([\sum_{i=1}^n (x_i - \bar{x})^4]/ns^4)$, where $\bar{x}$ and s are sample mean and standard deviation of $\{x_i\}_{i=1}^n$, respectively. If $\kappa_x > 3$, the empirical distribution of $\{x_i\}_{i=1}^n$ exhibits tails that are heavier than those of a Gaussian distribution. Consequently, we interpret a large κ_x value as compelling evidence of movements within the signals. In our experiments, we set an empirical threshold of 5 to detect movement-affected signals when an individual is asleep.

4) Heartbeat Detection and HR Estimation: Certain signals captured from the bed, while free from movement, may still lack a discernible heartbeat, as depicted in the bottom row of Fig. 8. It is crucial to exclude these types of signals to prevent errors in the estimation of vital signs. Following the quality assessment steps mentioned earlier, if a signal is deemed high quality, it then serves as the basis for calculating HR, RR, and IBI.

Our HR estimation is closely tied to the heartbeat detection method. A significant challenge in our HR estimation algorithm is the intricate waveform shape of each heartbeat cycle. This waveform harbors a degree of randomness which could introduce inaccuracies in HR determination. To address this, we extract the envelope of the heartbeat cycle, a smoother version of the waveform, to calculate HR. This envelope, with its reduced noise, presents a periodicity that is more readily identifiable. Guided by this understanding, we outline a four-step signal processing approach for HR estimation. The efficacy of this method is further showcased in Fig. 9.

Step 1: To retrieve the envelope of the signal, we employ the Hilbert transform as described in [40]. The transform operates under the assumption that a signal's amplitude is modulated by its instantaneous amplitude (envelope) as given by the equation $x(t) = a(t) \cdot \cos(\omega t)$, where $x(t)$ is the raw signal and $a(t)$ is the envelope that we aim to extract from $x(t)$. The Hilbert transform calculates the imaginary part $x_i(t)$ of a real signal $x(t)$ using the relation $x_i(t) = HT[x(t)]$, where $HT[\cdot]$ represents the Hilbert transform operator. An analytic signal $z(t)$ can be formed using the real signal $x(t)$ and its Hilbert-transformed counterpart $x_i(t)$ $z(t) = x(t) + i \cdot x_i(t)$. The envelope $a(t)$ is then derived as $a(t) = \sqrt{x^2(t) + x_i^2(t)}$.

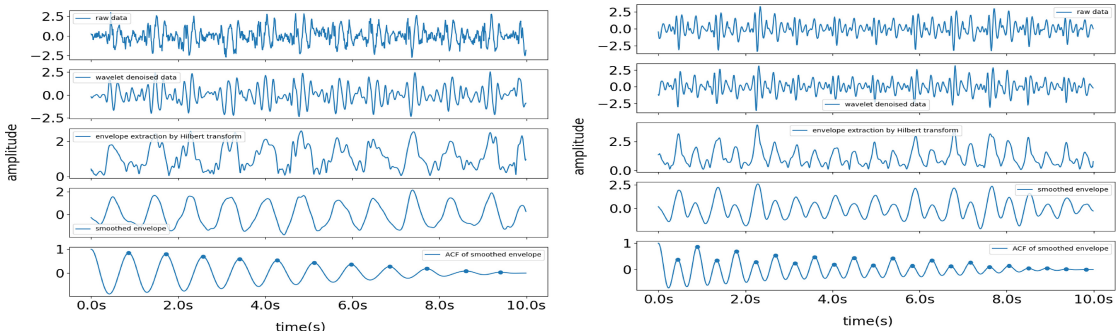

Fig. 9. Procedure for detecting heartbeat of the signal by obtaining ACF from a smoothed envelope of signal (Left). Signal that contains two peaks within one heartbeat cycle (Right).

Step 2: To enhance the envelope of the signal, we incorporate a Savitzky–Golay filter [41]. The Savitzky–Golay filter, based on least squares, is essentially a polynomial smoothing filter. It derives filter coefficients by minimizing the discrepancy between the raw and the filtered data. The crucial parameters that need adjustment are the window size (W) and the polynomial order (N). The filter's coefficients are derived by aiming to minimize the equation

$$\mathcal{E}_N = \sum_{n=-M}^{M} \left(\sum_{k=0}^{N} a_k n^k - x[n] \right)^2$$

where $2 \cdot M + 1 = W$, and the expression $\sum_{k=0}^{N} a_k n^k$ offers a polynomial approximation corresponding to $x[n]$. For each window, filter coefficients are determined for the central point. Subsequently, the window is shifted to the right by a single point, and the same procedure is reiterated to pinpoint the next central point within this window. This iterative process yields a more refined version of the data, preserving its essential characteristics and diminishing noise. The spikes in the extracted envelope represent swift alterations in signal amplitude, often stemming from noise or other signal artifacts. The Savitzky–Golay filter, by smoothing these spikes, fortifies the precision of the ensuing processing steps.

Step 3: To discern the periodicity of the smoothed envelope, we employ its ACF, a widely utilized function in time series analysis. the ACF calculates the correlation between the envelope at time t and that at time $t + k$; thereby elucidating the signal's periodicity. The lag-k autocorrelation for $\{x_i\}_{i=1}^{n}$ is defined as $\text{ACF}(k) = ([\sum_{i=1}^{n-k}(x_i - \bar{x})(x_{i+k} - \bar{x})]/[\sum_{i=1}^{n}(x_i - \bar{x})^2])$. In a signal that remains stationary and periodic, both its mean and variance tend to be consistent. To ascertain whether a signal is periodic, we segment it into uniform-length portions and set a threshold 0.1 on the variance of these segments' mean. If the variance of the mean is beneath the prescribed threshold, it suggests that the signal fulfills one of the prerequisites for periodicity.

Step 4: We transition to the frequency domain of the ACF by determining its power spectral density (PSD) through Welch's method [42]. Welch's approach involves estimating a windowed PSD from overlapping segments of the signal. By averaging these windowed PSDs, the final PSD becomes smoother and more robust. Specifically, the windowed PSD can be conceptualized as the fast FFT of a signal segment, further multiplied by a window function, such as the Hamming function. It is imperative to note that the dominant frequency component of the ACF should lie between 0.6 and 3 Hz, a range that encapsulates the typical heartbeat frequency for humans. Additionally, the magnitude of this maximum frequency peak ought to surpass a predetermined autocorrelation lower bound, like 0.1, ensuring differentiation from random noises. A segment is deemed to harbor a rich periodic signal apt for vital sign estimation if it fulfills both these frequency and magnitude criteria.

Traditionally, HR is estimated by counting the number of heartbeats in a signal. However, this method can be unstable in real-time monitoring contexts. Consider a scenario where the actual HR of a participant is 60 beats per minute (bpm). In a 10-s signal, missing or adding just one heartbeat can lead to an estimation error exceeding 10% for HR. To address this, one might employ the median of heartbeat intervals, providing a more robust alternative for HR estimation. However, errors can arise when the incoming signal displays two distinct peaks within a single heartbeat cycle, as illustrated on the right side of Fig. 9. The first of these peaks is termed the systolic peak, while the second is the diastolic peak. The presence of both these peaks in the ACF might result in double-counting errors, causing the estimated HR to be nearly twice the actual HR. To address this, it is crucial to disregard the ACF peaks representing the autocorrelation between the systolic and diastolic peaks within each heartbeat cycle.

Building on the insights from [37], we integrate the frequency domain features of the smoothed envelope, derived from step 2, with the ACF, viewing the ACF as a time domain attribute. We narrow our focus to the pertinent region of the ACF. The frequency domain features are ascertained using Welch's method. To morph the aforementioned features into probability density functions (PDFs), we deploy a softmax transformation: $\sigma(x_i) = (e^{x_i}/\sum_{j=1}^{N} e^{x_j})$, where x_i represents the ith data point in a segment signal x, $\sigma(\cdot)$ denotes the softmax operation, and N is the aggregate count of data points in segment x. To fuse these two features, we leverage probabilistic Bayesian reasoning. First, the spectrum generated through Welch's method can be construed as "the likelihood of frequency (f) being the genuine fundamental frequency, given the spectrum": $P(f|\text{spectrum})$. Concurrently, the ACF can be interpreted as "the probability of a specific quantity of data points (n) representing the genuine periodicity, given the

ACF": $P(n|\text{ACF})$. Each feature assigns a "probability" denoting the likelihood of each potential input (f or n) being the "true" value. Now, with two independent PDFs at hand, our objective is to pinpoint the most probable outcomes under the amalgamation of these PDFs. We can substitute f with n in $P(f|\text{spectrum})$, as $n = (Fs/f)$, to establish a joint distribution: $P(n|\text{spectrum, ACF})$.

Consequently, our mission centers on discerning the most probable value for n when considering both the spectrum and ACF combined, i.e.,

$$n = \arg\max_n P(n|\text{spectrum, ACF}). \tag{2}$$

In light of Bayes' theorem and assuming the two features are independent conditioning on n, we have

$$\begin{aligned} &P(n|\text{spectrum, ACF}) \\ &\propto P(n) \cdot P(\text{ACF}|n) \cdot P(\text{spectrum}|n) \\ &= P(n|\text{ACF}) \cdot P(\text{ACF}) \cdot \frac{P(n|\text{spectrum}) \cdot P(\text{spectrum})}{P(n)} \\ &\propto \frac{P(n|\text{spectrum}) \cdot P(n|\text{ACF})}{P(n)}. \end{aligned}$$

Assuming $P(n)$ adheres to a uniform distribution is reasonable, as we do not privilege any particular value of n. This allows us to further simplify the objective function by dropping $P(n)$. Ultimately, we have

$$P(n|\text{spectrum, ACF}) \propto P(n|\text{spectrum}) \cdot P(n|\text{ACF}). \tag{3}$$

Subsequently, the "optimal" choice of n—representing the most probable periodicity of the incoming signal—can be discerned by identifying the peak output from the joint distribution of spectrum and ACF, $P(n|spectrum, ACF)$, in accordance with (3). Let Fs symbolize the signal's sampling rate and let n denote the true periodicity with the highest probability. We suggest a robust HR estimation as $\text{HR} = (60/n) \cdot Fs$, with $n = \text{argmax}_n(P(n|\text{spectrum}) \times P(n|\text{ACF}))$.

B. IBI Estimation

While IBI estimation is closely tied to HR estimation, directly perform detection of heartbeat peaks can result in numerous false identifications. This is because the pivotal step in IBI estimation revolves around pinpointing every heartbeat peak position. Directly identifying heartbeat peaks on raw data or data post-wavelet denoising can introduce significant errors. Furthermore, our primary aim is to compute the intervals between consecutive heartbeats. Therefore, the difference between two consecutive peaks hold more relevance than the precise peak positions. With this perspective, we suggest pinpointing the peak positions on the ACF and subsequently estimating IBI as delineated below.

Step 1: First, we estimate the signal's average IBI. We then determine the position of the first heartbeat peak (P_1) by identifying the location of the peak with the highest amplitude in the ACF of the signal, confined within the range $[0, N]$. Here, $N = IBI \cdot Fs$ represents the data point count for the average IBI.

Step 2: Upon determining the first heartbeat peak, we recalibrate the starting and concluding indices of the sliding window.

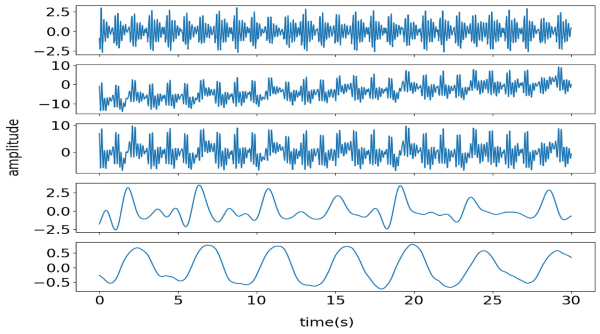

Fig. 10. From top to down. (1) Raw data. (2) Respiration pattern revealed signal from (1). (3) Detrended data from (2). (4) Wavelet denoised data of (3). (5) Moving average of (4).

The revised start index is set to $P_1 + 0.75 \cdot N$, whereas the updated end index becomes $P_1 + N + c$. Here, c is a minimal positive constant, ensuring the presence of a heartbeat peak in the search window, especially considering the rare scenarios where certain peak intervals might exceed the average IBI for a specific signal segment.

Step 3: Step 2 is reiterated until the end index surpasses the signal's length, all the while making sure the start index remains within the confines of the signal's length. Subsequently, we examine the signal for any lingering peaks. If identified, we determine the peak position with the utmost amplitude. If no peaks are discernible, we deduce that all heartbeat peaks have been successfully detected.

Step 4: Once all heartbeat peaks, represented as $P = [p_1, \ldots, p_N]$, are detected, we proceed to calculate IBIs for this signal segment as $IBIs = [(p_2 - p_1), \ldots, (p_N - p_{N-1})]$.

C. RR Estimation

Separating breathing cycles from heartbeats in raw signals is particularly challenging because the velocity of vibrations induced by respiration is substantially slower than that instigated by heartbeats. Consequently, a single breathing cycle can encompass several heartbeats, complicating its detection within brief signal durations. As illustrated in Fig. 10, the top row displays a 30-s signal where the heartbeats are clear but breathing cycles are hard to be visually identified. To address this challenge, we obtain displacement data by integrating the raw velocity data. This methodology aids in unveiling the respiration pattern embedded within the raw data. Nevertheless, the output from the geophone is nearly proportional to velocity, rather than representing a true velocity. The geophone can produce outputs even in the absence of vibrations, attributed to intrinsic errors within its system.

For a time-step i, let x_i be the output of the geophone, v_i be the true velocity, and e_i be a Gaussian error with mean μ and variance σ^2. We model the output of geophone as $x_i = C \cdot v_i + e_i$. By subtracting the expectations from both sides, we have $\hat{x}_i = C \cdot \hat{v}_i + \hat{e}_i$ with

$$\hat{x}_i = x_i - E[x_i], \;\; \hat{v}_i = v_i - E[v_i], \;\; \text{and } \hat{e}_i \sim N\left(0, \sigma^2\right).$$

In the context of RR estimation, the amplitude of the signal is not our primary concern. Instead, we focus on the waveform of the signal. As a result, C can be treated as 1 in this scenario.

Fig. 11. Caretaker4 Device.

Fig. 12. Sleep monitoring GUI, that is able to visualize vital signs, such as HR and RR.

This leads us to the relationship $\hat{x}_i = \cdot\hat{v}_i + \hat{e}_i$. Subsequently, we propose to unveil the respiration pattern by

$$D_T = \int_{t=1}^{T} \hat{x}_t dt = \int_{t=1}^{T} \hat{v}_t dt + \int_{t=1}^{T} \hat{e}_t dt$$
$$\text{or} \quad D_T = \sum_{i=1}^{T} \hat{x}_i = \sum_{i=1}^{T} \widehat{v_i} + \sum_{i=1}^{T} \widehat{e_i} \tag{4}$$

where D_T is the displacement at the time step T. Then, we substitute $\sum_{i=1}^{T} \hat{v}_i$ and $\sum_{i=1}^{T} \hat{e}_i$ with y_T and b_T

$$D_T = y_T + b_T \text{ with } b_T \sim N\left(0, T \cdot \sigma^2\right) \tag{5}$$

where y_T is defined as the sum of heartbeat displacement hd_T and respiration displacement rd_T at time T. The latter rd_T represents the target signal we aim to recover: $D_T = hd_T + rd_T + b_T$. From (5), it is evident that the variance of the internal error grows over time. Despite this, after executing the aforementioned operations, the respiration pattern becomes discernible, as illustrated in Fig. 10. The breathing pattern is clearly visible in the second row of Fig. 10. However, there is baseline wandering due to the system error, indicating the need for detrending.

Moreover, we utilize wavelet denoising to eliminate the interference from hd_T, leaving only the signals associated with rd_T and b_T. To further extract rd_T, we implement a moving average filter with substantially large window size. This decision is grounded in the understanding that $E[rd_T + b_T] = E[rd_T] + E[b_T] = E[rd_T]$. Under the premise that the respiration signal is deterministic, it is reasonable to infer that $E[rd_T] = rd_T$. The comprehensive process of extracting rd_T is depicted in Fig. 10, where the bottom panel presents the final rd_T.

We extract the breathing signal rd_T and compute its ACF. To enhance the robustness of the RR estimation, we employ a feature fusion strategy akin to that used in HR estimation. We determine the ACF on the wavelet-denoised signal ($rr_{\text{wav}} = rd_T + b_T$) and on the detrended signal (rr_{sg}) post-application of the Savitzky–Golay filter (as seen in the third row of Fig. 10). These three features are then merged to produce a final PDF for the fused ACF. This PDF can be expressed as $P(n|\text{ACF}_{rd_T}, \text{ACF}_{rr_{\text{wav}}}, \text{ACF}_{rr_{sg}}) \propto P(n|\text{ACF}_{rd_T}) \cdot P(n|\text{ACF}_{rr_{\text{wav}}}) \cdot P(n|\text{ACF}_{rr_{sg}})$. We then estimate RR by pinpointing the most prominent peak within a range of 2 to 10 s on the PDF of the fused ACF. Such a methodology proves especially valuable in counteracting the over-filtering of the breathing signal, given instances where rr_{sg} and rr_{wavelet} retain a more accurate shape compared to rd_T.

IV. Experiment Setup and Evaluation

BedDot can be installed using its mounted magnetic, allowing for easy deployment on standard beds or seats without necessitating any special modifications. In our experiments, we tested the device on a hospital bed and a seat within a hospital setting, as well as on a regular bed in a residential setting, to simulate real-life conditions. Each bed was equipped with a BedDot positioned beneath the chest region. For the HR and RR benchmarks, we relied on the commercially available, FDA-approved Caretaker4 device as our point of reference. Caretaker 4, as depicted in Fig. 11, is designed to provide continuous estimations of vital signs, such as HR and RR by analyzing the pulse pressure waveform obtained from a wireless finger sensor. The device employs controlled air pressure to the attached finger to capture this pulse pressure waveform. We gathered data from 75 participants who were instructed to lie in various postures, including on their back, stomach, and both sides. Subsequently, participants were prompted to take short nap to simulate genuine sleep scenarios. Throughout the experiment, various motions resulting from unintentional body shifts, deliberate position changes, or other external disturbances often obscured the heartbeat within the noise. After implementing a signal quality assessment algorithm capable of vital sign estimation, our final data set comprised 28 494 distinct observations collected from the 75 participants over a span of 80 h. Participants' ages varied around a mean of 50 ± 19 years, consisting of 32 males and 43 females. On average, their heights measured 167 ± 9 cm, with average weights of 81 ± 19 kg.[1]

To illustrate sleep status, we designed a graphical user interface (GUI) leveraging the Grafana tool [43], as depicted in Fig. 12. The upper panel showcases real-time HR and RR values, while a blue box in the top-left corner signifies the bed's active or inactive status. The lower panel presents the raw data gathered from participants in real time. Additionally, this GUI offers insights into historical HR/RR data, body movement patterns, posture transitions, and bed statuses, making it suitable for both live monitoring and retrospective analysis of historical records.

For the evaluation, we initially compare the proposed vital sign estimation techniques with a baseline method. This baseline focuses on the HR, RR [21], [38], and IBI estimations [37] as delineated in Section II-B. When assessing HR and IBI, we employed 10-s data segments for comparative analysis. For

[1]The clinical experiments were approved by IRB PROJECT00001838.

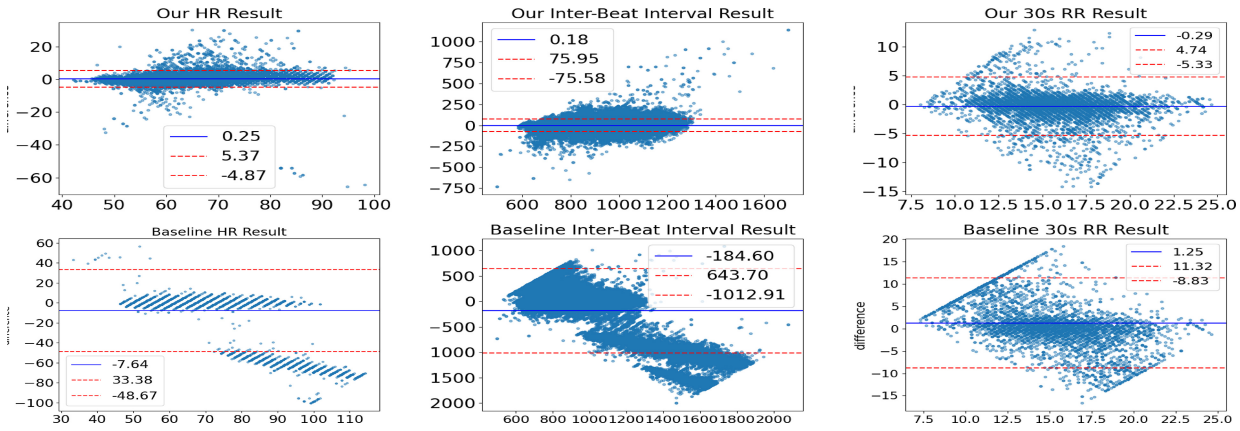

Fig. 13. Bland Altman Analysis for HR (left), RR (right), and IBI (middle) estimation by the proposed algorithm (top) and baseline method (bottom). For all figures, x axis is the average between ground-truth and predictions. Y axis is the difference between ground-truth and predictions.

TABLE I
COMPARISON BETWEEN PROPOSED ALGORITHMS AND BASELINE METHODS ON HR, IBI, AND RR ESTIMATION

METHOD	VITAL	MAE	MAPE	STD
PROPOSED ALGORITHM	**HR(BPM)**	1.38	0.0211	2.22
	30s RR(BPM)	1.54	0.1076	2.00
	IBI(ms)	24.84	0.0273	29.62
BASELINE METHOD	**HR(BPM)**	8.76	0.1378	20.49
	30s RR(BPM)	3.13	0.2149	3.40
	IBI(ms)	218.06	0.2532	402.59

RR, we utilized 30-s segments for evaluation and comparison. Subsequent to this, we assessed bed occupancy results. We further examined HR, RR, IBI, and bed occupancy under various conditions and settings, encompassing hospital beds, residential beds in assorted postures, and seats. This assessment included presenting the MAE for each individual pertaining to HR, RR, and IBI estimations. Concluding our evaluation, we gauged the effectiveness of our signal quality assessment algorithm by contrasting HR and RR outcomes across data sets—both prior to and following the application of the signal quality assessment algorithm. We disclosed the MAE, the standard deviation of the absolute error (STD), and the mean absolute error percentage (MAPE) for HR, RR, and IBI estimations. The mean absolute percentage error is articulated as $\text{MAPE} = (1/n)\sum_{i=1}^{n} |(\text{label}_i - \text{prediction}_i/\text{label}_i)|$.

A. Comparison of HR, IBI, and RR Estimation Between the Proposed Algorithm and Baseline Method

The outcomes for HR estimation are showcased in Fig. 13. It becomes clear that our proposed algorithm aligns more closely with the true labels and exhibits significantly reduced error variance in comparison to the baseline approach. The majority of predictions from our model align closely with the true labels, underlining the reliability of our HR estimation method. Detailed statistical results from the proposed HR estimation method are provided in Table I. These results align with the AAMI standard, which necessitates an MAE within 5 BPM and an MAPE under 10% for cardiac monitors and HR meters [44]. Notably, our proposed HR estimation techniques surpass the baseline in measures of MAE, STD, and MAPE.

Next, we assessed the IBI outcomes against the benchmark labels procured from an FDA-approved device, contrasting them with the baseline method presented in [37]. This was essential, as prior geophone-based systems lacked the capability to estimate IBI [21], [38]. The findings, presented in Fig. 13, underscore the enhanced stability of our proposed algorithm in relation to the baseline method. This is evident from the predictions that closely mirror the true labels. We also detail the statistical results for the IBI estimation in Table I. Evidently, our IBI estimation method surpasses the baseline technique, setting a new benchmark in metrics like MAE, MAPE, and the standard deviation of error. It is worth noting that the baseline method from [37] requires considerably more time to process each data sample in comparison to our proposed method.

The outcomes for RR estimation using 30-s data segments are depicted in Fig. 13. These results illustrate that the proposed methodology offers both a lower MAE and reduced variance in errors when juxtaposed with the baseline approach. As corroborated by the results in Table I, our advanced RR estimation algorithm exhibits superior performance to the baseline RR estimation strategy, especially in metrics, such as MAE, STD, and MAPE, when applied to 30-s data.

B. Comparison of HR, IBI, and RR Estimation Between the Proposed Algorithm and Algorithms Based on Other Types of Bed Sensors

We opted to evaluate the HR estimation algorithm and the respiration rate estimation algorithm from [10] and [33] alongside the IBI estimation algorithm from [37], which was assessed earlier in Section IV-A. Noted that the sensor used in [33] incorporates a cost effective, commercial load cell, which operates as a force sensor. The sensor in [10] is predicated upon a microbend fiber optic structure. Moreover, [37] employs a singular electromechanical-film (EMFi) sensor. Notably, the HR estimation techniques described in both [10] and [33] were found to be ineffective when tested on our data set. For an in-depth comparison of these results, readers are directed to Table II.

C. Bed Occupancy Evaluation

Bed occupancy is assessed using metrics, such as accuracy, recall, specificity, and precision. The associated confusion matrix is presented in Fig. 14. Within this context, a positive

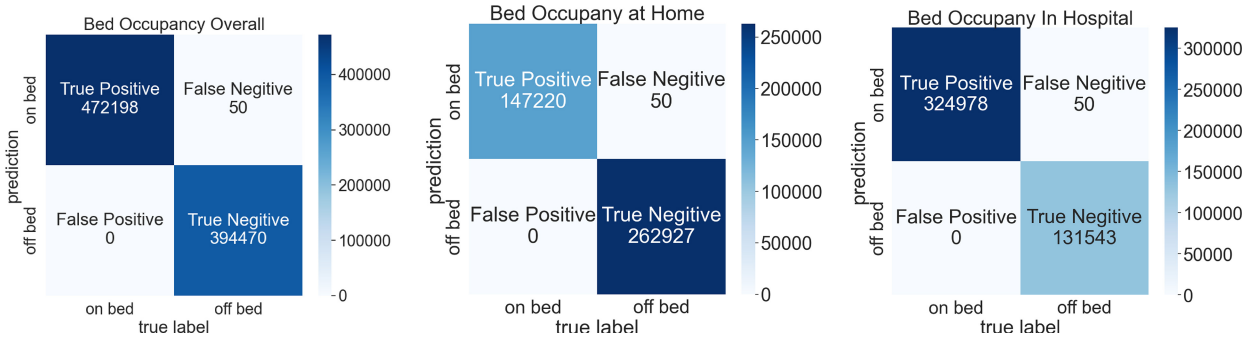

Fig. 14. Confusion matrix of overall bed occupancy (left), on home (middle), and hospital (right).

TABLE II
HR AND RR ESTIMATION COMPARISON AGAINST OTHER ALGORITHMS ON OTHER TYPES OF SENSORS

METHOD	VITAL	MAE	MAPE	STD
[33]	**HR(BPM)**	49.17	0.7870	59.76
	RR(BPM)	3.52	0.2139	2.42
[10]	**HR(BPM)**	22.66	0.3437	33.36
	RR(BPM)	5.53	0.4047	4.35
PROPOSED	**HR(BPM)**	1.38	0.0211	2.22
	RR(BPM)	1.54	0.1076	2.00

TABLE III
BED OCCUPANCY RESULT OVERALL AND ON DIFFERENT ENVIRONMENTS

Environments	Accuracy	Recall	Specificity	Precision
Home	99.99%	99.97%	100%	100%
Hospital	100%	100%	100%	100%
Overall	99.99%	99.99%	100%	100%

result signifies on-bed, while a negative indicates off-bed. The comprehensive results, covering accuracy, sensitivity, specificity, precision, and recall, are displayed in the bottom row of Table III, with each metric nearly reaching the 100% mark. The system provides bed occupancy detection results in real time, every second, based on a 10-s segment with a 30-s moving average window. The evaluations draw upon data gathered from 75 individuals. Moreover, we further assessed ten consecutive days and nights in real-world scenarios involving ten participants. Data from each day encompasses daily activities—excluding sleep data but inclusive of daily events around the bed and ambient noise—alongside sleep data.

D. Evaluation on Different Environments

The preceding sections have showcased the adaptability of our algorithms across diverse individuals. In this section, we further assess the robustness and versatility of our vital sign estimation and bed occupancy algorithms across varied environments. We specifically evaluate the performance of the HR, RR, and IBI estimation, as well as the bed occupancy algorithms, in both home and hospital settings. Additionally, by testing and evaluating the HR, RR, and IBI estimation algorithms on a seat, we highlight their potential for integration into smart office environments.

TABLE IV
HR, RR, AND IBI ESTIMATION ON DIFFERENT CONDITIONS

CONDITIONS	VITAL	MAE	MAPE	STD
HOME	**HR(BPM)**	1.33	0.0203	2.06
	30s RR(BPM)	1.34	0.0930	1.65
	IBI(ms)	25.99(ms)	0.0283	31.25
HOSPITAL	**HR(BPM)**	1.41	0.0226	2.51
	30s RR(BPM)	2.02	0.1433	2.33
	IBI(ms)	22.93(ms)	0.0255	26.55
SEAT	**HR(BPM)**	1.18	0.0182	0.89
	30s RR(BPM)	1.43	0.1157	1.22
	IBI(ms)	30.22(ms)	0.0336	31.82(ms)

1) HR, RR, and IBI Estimation on Different Environments and Seat: In this section, we assess the performance of our vital sign estimation algorithms across various platforms: a hospital bed, a family bed, and a chair or seat, to validate the adaptability of our methodologies. The outcomes are documented in Table IV. For IBI estimation, the results from the hospital bed slightly outperform those from the family bed. However, for HR and RR estimations, the algorithms exhibit superior performance on the family bed as compared to the hospital bed and seat. Overall, the estimation of vital signs remains commendable across all settings, underscoring the broad applicability of our algorithm.

2) Bed Occupancy in Home Environment and Hospital Environment: In this section, we analyze the efficacy of our bed occupancy algorithm across two distinct settings: 1) home and 2) hospital. These evaluations span a period of five days for each environment. The associated confusion matrices are depicted in Fig. 14.

The first two rows of Table III present the outcomes of the bed occupancy estimation across varied environments. Notably, false positives, indicating on bed, were observed solely in the home environment. Upon closer examination, we discerned that the segments with these false positives bore resemblances to the heartbeat signal, complicating their differentiation even upon visual inspection.

E. Evaluation of HR, RR, and IBI Estimation on Different Postures

In this section, we assess the estimations of HR, RR, and IBI across various postures: lying on the back, left side, right side, and stomach. The evaluation outcomes, as depicted in

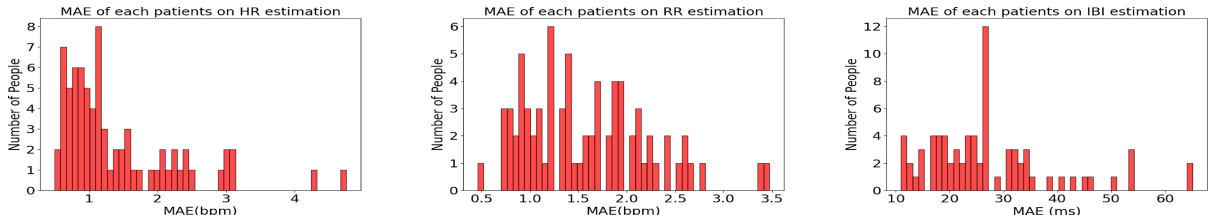

Fig. 15. Histograms of MAE for HR, RR, and IBI estimation errors over all subjects.

TABLE V
HR, RR, AND IBI ESTIMATION ON DIFFERENT POSTURES

CONDITIONS	VITAL	MAE	MAPE	STD
BACK	**HR(BPM)**	1.17	0.0178	1.97
	30s RR(BPM)	1.83	0.1276	1.99
	IBI(ms)	26.36(ms)	0.0291	31.02
LEFT	**HR(BPM)**	1.11	0.0181	1.91
	30s RR(BPM)	1.60	0.1296	2.15
	IBI(ms)	25.37(ms)	0.0275	27.65
RIGHT	**HR(BPM)**	1.10	0.0159	1.20
	30s RR(BPM)	2.65	0.1801	2.81
	IBI(ms)	24.71(ms)	0.0299	33.37
STOMACH	**HR(BPM)**	1.40	0.0203	2.63
	30s RR(BPM)	1.21	0.0743	0.94
	IBI(ms)	21.40(ms)	0.0261	24.88

TABLE VI
PERFORMANCE OF SIGNAL QUALITY ASSESSMENT

Accuracy	Recall	Specificity	Precision
95.63%	96.08%	95.19%	95.14%

Table V, affirm that our vital signs algorithm is versatile and accommodates all these postures effectively.

F. Evaluation of HR, RR, and IBI Estimation Across Different Patients

Histograms presented in Fig. 15 depict the empirical distribution of individuals across varying error ranges for HR, RR, and IBI estimations. These histograms indicate that there are minimal substantial errors associated with any subject for HR, RR, and IBI estimations. While a few outliers exhibit higher estimation errors, the errors for the vast majority of subjects are closely clustered, underscoring the robustness of both the BedDot system and the proposed vital sign estimation methods.

G. Performance for Signal Quality Assessment Algorithm on Signal Quality Detection

We provided manual signal quality labels from 50 patients. Those lacking distinct heartbeats were marked as "low-quality data," while the rest were deemed "high-quality data." The effectiveness of our signal quality assessment algorithm is demonstrated through the results in Table VI.

H. Evaluation for Effect of Signal Quality Assessment

To evaluate our signal quality assessment algorithm, we compared HR and RR performance using two data sets: one prior to implementing the algorithm and another after. Initial results, presented in Table VII, showed suboptimal HR and RR estimation, as evident in Table I. Upon applying our algorithm, we observed substantial enhancements in accuracy and stability, as demonstrated by reduced MAE, MAPE, and STD values. These improvements underscore our algorithm's role in elevating signal quality for more precise HR and RR estimates. Our vital sign estimation algorithm, without signal quality assessment, computes vital signs for all available data during bed occupancy. Conversely, the incorporation of the signal quality assessment algorithm effectively identifies and filters out segments with substantial movements that distort signal waveforms. Additionally, segments lacking clear heartbeat patterns are systematically excluded. Consequently, 75% of the collected data, with a detection rate (DR) of 75%, now yield accurate vital sign estimations. Detailed outcomes are documented in Table VII.

TABLE VII
EFFECT OF SIGNAL QUALITY ASSESSMENT ALGORITHM

VITAL	MAE	MAPE	STD
HR(BPM)	5.46(↑ 4.08)	0.0795(↑ 0.0584)	9.71(↑ 7.49)
30s RR(BPM)	2.50(↑ 0.96)	0.1758(↑ 0.0682)	2.76(↑ 0.76)

V. CONCLUSION

In this article, we introduce BedDot, a contactless bedside system for real-time monitoring of HR, RR, and IBI, alongside accurate bed occupancy detection during sleep. Our experiments demonstrate its efficacy across various conditions. BedDot is cost effective, easily installable, and offers real-time vital sign and occupancy status visualization through our user-friendly GUI. Our signal quality assessment algorithm enhances vital sign estimation by identifying bed occupancy and filtering distorted signals. Our vital sign estimation algorithms perform well, evidenced by their MAE, STD, and MAPE values, and exhibit versatility across diverse conditions. The system holds potential for clinical or home use. Our current exploration of vital signs estimation has been focused on a single individual. Future work will extend to multiperson scenarios and includes AF detection and stress analysis. Furthermore, we plan to expand monitoring beyond in-bed sleep to include seat monitoring during daily activities.

ACKNOWLEDGEMENT

The authors thank Stephanie Croyle, Kimberly Schmitz, and all UGA CTRU staff for helping the IRB and data collection experiments.

REFERENCES

[1] R. N. Aurora, S. P. Patil, and N. M. Punjabi, "Portable sleep monitoring for diagnosing sleep apnea in hospitalized patients with heart failure," *Chest*, vol. 154, no. 1, pp. 91–98, 2018.

[2] A. A. Khan, G. Y. Lip, and A. Shantsila, "Heart rate variability in atrial fibrillation: The balance between sympathetic and parasympathetic nervous system," *Eur. J. Clin. Investig.*, vol. 49, no. 11, 2019, Art. no. e13174.

[3] H.-G. Kim, E.-J. Cheon, D.-S. Bai, Y. H. Lee, and B.-H. Koo, "Stress and heart rate variability: A meta-analysis and review of the literature," *Psychiatr. Investig.*, vol. 15, no. 3, p. 235, 2018.

[4] Á. Jobbágy, M. Majnár, L. K. Tóth, and P. Nagy, "HRV-based stress level assessment using very short recordings," *Period. Polytech. Electr. Eng. Comput. Sci.*, vol. 61, no. 3, pp. 238–245, 2017.

[5] G. Y. Lui, D. Loughnane, C. Polley, T. Jayarathna, and P. P. Breen, "The apple watch for monitoring mental health–related physiological symptoms: Literature review," *JMIR Ment. Health*, vol. 9, no. 9, 2022, Art. no. e37354.

[6] S. Tedesco et al., "Validity evaluation of the Fitbit Charge2 and the Garmin vivosmart HR+ in free-living environments in an older adult cohort," *JMIR mHealth uHealth*, vol. 7, no. 6, 2019, Art. no. e13084.

[7] C. Paradiso, F. Colino, and S. Liu, "The validity and reliability of the Mi band wearable device for measuring steps and heart rate," *Int. J. Exerc. Sci.*, vol. 13, no. 4, p. 689, 2020.

[8] B. Fang, N. D. Lane, M. Zhang, A. Boran, and F. Kawsar, "BodyScan: Enabling radio-based sensing on wearable devices for contactless activity and vital sign monitoring," in *Proc. 14th Annu. Int. Conf. mobile Syst., Appl., Serv.*, 2016, pp. 97–110.

[9] T. Hao, C. Bi, G. Xing, R. Chan, and L. Tu, "MindfulWatch: A smartwatch-based system for real-time respiration monitoring during meditation," *Proc. ACM Interact. Mob. Wearable Ubiquitous Technol.*, vol. 1, no. 3, pp. 1–19, 2017.

[10] I. Sadek, E. Seet, J. Biswas, B. Abdulrazak, and M. Mokhtari, "Nonintrusive vital signs monitoring for sleep apnea patients: A preliminary study," *IEEE Access*, vol. 6, pp. 2506–2514, 2017.

[11] J. H. Shin, Y. J. Chee, D.-U. Jeong, and K. S. Park, "Nonconstrained sleep monitoring system and algorithms using air-mattress with balancing tube method," *IEEE Trans. Inf. Technol. Biomed.*, vol. 14, no. 1, pp. 147–156, Jan. 2010.

[12] Y. Zhu, J. Maniyeri, V. F. S. Fook, and H. Zhang, "Estimating respiratory rate from FBG optical sensors by using signal quality measurement," in *Proc. 37th Annu. Int. Conf. IEEE Eng. Med. Biol. Soc. (EMBC)*, 2015, pp. 853–856.

[13] M. Krej, Ł. Dziuda, and F. W. Skibniewski, "A method of detecting heartbeat locations in the ballistocardiographic signal from the fiber-optic vital signs sensor," *IEEE J. Biomed. Health Inform.*, vol. 19, no. 4, pp. 1443–1450, Jul. 2015.

[14] T. Rahman et al., "Dopplesleep: A contactless unobtrusive sleep sensing system using short-range doppler radar," in *Proc. 2015 ACM Int. Joint Conf. Pervasive Ubiquitous Comput.*, 2015, pp. 39–50.

[15] J. Liu, Y. Chen, Y. Wang, X. Chen, J. Cheng, and J. Yang, "Monitoring vital signs and postures during sleep using WiFi signals," *IEEE Internet Things J.*, vol. 5, no. 3, pp. 2071–2084, Jun. 2018.

[16] Y. S. Lee, P. N. Pathirana, T. Caelli, and R. Evans, "Doppler radar in respiratory monitoring: Detection and analysis," in *Proc. Int. Conf. Control, Autom. Inf. Sci. (ICCAIS)*, 2013, pp. 224–228.

[17] N. Molinaro, E. Schena, S. Silvestri, and C. Massaroni, "Multi-ROI spectral approach for the continuous remote cardio-respiratory monitoring from mobile device built-in cameras," *Sensors*, vol. 22, no. 7, p. 2539, 2022.

[18] M. van Gastel, S. Stuijk, S. Overeem, J. P. van Dijk, M. M. van Gilst, and G. de Haan, "Camera-based vital signs monitoring during sleep–A proof of concept study," *IEEE J. Biomed. Health Inform.*, vol. 25, no. 5, pp. 1409–1418, May 2021.

[19] C. Yang, M. Hu, G. Zhai, and X.-P. Zhang, "Graph-based denoising for respiration and heart rate estimation during sleep in thermal video," *IEEE Internet Things J.*, vol. 9, no. 17, pp. 15697–15713, Sep. 2022.

[20] Z. Yang, P. H. Pathak, Y. Zeng, X. Liran, and P. Mohapatra, "Vital sign and sleep monitoring using millimeter wave," *ACM Trans. Sensor Netw. (TOSN)*, vol. 13, no. 2, pp. 1–32, 2017.

[21] Z. Jia et al., "Monitoring a person's heart rate and respiratory rate on a shared bed using geophones," in *Proc. 15th ACM Conf. Embedded Netw. Sensor Syst.*, 2017, pp. 1–14.

[22] M. Pouliot, V. Joshi, R. Goubran, and F. Knoefel, "Bed occupancy monitoring: Data processing and clinician user interface design," in *Proc. Annu. Int. Conf. IEEE Eng. Med. Biol. Soc.*, 2012, pp. 5810–5814.

[23] M. Taylor, T. Grant, F. Knoefel, and R. Goubran, "Bed occupancy measurements using under mattress pressure sensors for long term monitoring of community-dwelling older adults," in *Proc. IEEE Int. Symp. Med. Meas. Appl. (MeMeA)*, 2013, pp. 130–134.

[24] A. Braun, M. Majewski, R. Wichert, and A. Kuijper, "Investigating low-cost wireless occupancy sensors for beds," in *Proc. 4th Int. Conf., Distrib., Ambient Pervasive Interact.:* Toronto, ON, Canada, Jul. 2016, pp. 26–34.

[25] J. Clemente, M. Valero, F. Li, C. Wang, and W. Song, "Helena: Real-time contact-free monitoring of sleep activities and events around the bed," in *Proc. IEEE Int. Conf. Pervasive Comput. Commun. (PerCom)*, 2020, pp. 1–10.

[26] F. Li, M. Valero, J. Clemente, Z. Tse, and W. Song, "Smart sleep monitoring system via passively sensing human vibration signals," *IEEE Sensors J.*, vol. 21, no. 13, pp. 14466–14473, Jul. 2021.

[27] F. De Tommasi, C. Massaroni, M. A. Caponero, M. Carassiti, E. Schena, and D. L. Presti, "FBG-based mattress for heart rate monitoring in different breathing conditions," *IEEE Sensors J.*, vol. 23, no. 13, pp. 14114–14122, Jul. 2023.

[28] F. De Tommasi, D. L. Presti, M. A. Caponero, M. Carassiti, E. Schena, and C. Massaroni, "Smart mattress based on multi-point fiber Bragg gratings for respiratory rate monitoring," *IEEE Trans. Instrum. Meas.*, vol. 72, pp. 1–10, Dec. 2023, doi: 10.1109/TIM.2022.3232615.

[29] M. T. Bianchi, "Sleep devices: Wearables and nearables, informational and interventional, consumer and clinical," *Metabolism*, vol. 84, pp. 99–108, Jul. 2018.

[30] I. Sadek and B. Abdulrazak, "Contactless remote monitoring of sleep: Evaluating the feasibility of an under-mattress sensor mat in a real-life deployment," *Health Syst.*, to be published.

[31] T. Vogels, M. Van Gastel, W. Wang, and G. De Haan, "Fully-automatic camera-based pulse-oximetry during sleep," in *Proc. IEEE Conf. Comput. Vis. Pattern Recognit. Workshops*, 2018, pp. 1349–1357.

[32] G. De Haan and A. Van Leest, "Improved motion robustness of remote-PPG by using the blood volume pulse signature," *Physiol. Meas.*, vol. 35, no. 9, p. 1913, 2014.

[33] A. Albukhari, F. Lima, and U. Mescheder, "Bed-embedded heart and respiration rates detection by longitudinal ballistocardiography and pattern recognition," *Sensors*, vol. 19, no. 6, p. 1451, 2019.

[34] D. Friedrich, X. L. Aubert, H. Führ, and A. Brauers, "Heart rate estimation on a beat-to-beat basis via ballistocardiography-a hybrid approach," in *Proc. Annu. Int. Conf. IEEE Eng. Med. Biol.*, 2010, pp. 4048–4051.

[35] J. M. Kortelainen and J. Virkkala, "FFT averaging of multichannel BCG signals from bed mattress sensor to improve estimation of heart beat interval," in *Proc. 29th Annu. Int. Conf. IEEE Eng. Med. Biol. Soc.*, 2007, pp. 6685–6688.

[36] A. Vehkaoja, S. Rajala, P. Kumpulainen, and J. Lekkala, "Correlation approach for the detection of the heartbeat intervals using force sensors placed under the bed posts," *J. Med. Eng. Technol.*, vol. 37, no. 5, pp. 327–333, 2013.

[37] C. Brüser, S. Winter, and S. Leonhardt, "Robust inter-beat interval estimation in cardiac vibration signals," *Physiol. Meas.*, vol. 34, no. 2, p. 123, 2013.

[38] Z. Jia et al., "HB-phone: A bed-mounted geophone-based heartbeat monitoring system," in *Proc. 15th ACM/IEEE Int. Conf. Inf. Process. Sensor Netw. (IPSN)*, 2016, pp. 1–12.

[39] T. O'Haver. "Peak finding and measurement." 2019. [Online]. Available: PeakFindingandMeasurement.htm

[40] M. Klingspor. "Hilbert transform: Mathematical theory and applications to signal processing." 2015. [Online]. Available: https://www.diva-portal.org/smash/get/diva2:872439/FULLTEXT02

[41] A. Savitzky and M. J. Golay, "Smoothing and differentiation of data by simplified least squares procedures," *Anal. Chem.*, vol. 36, no. 8, pp. 1627–1639, 1964.

[42] P. Welch, "The use of fast fourier transform for the estimation of power spectra: A method based on time averaging over short, modified periodograms," *IEEE Trans. Audio Electroacoustics*, vol. AU-15, no. 2, pp. 70–73, Jun. 1967.

[43] M. Chakraborty and A. P. Kundan, "Grafana," in *Monitoring Cloud-Native Applications: Lead Agile Operations Confidently Using Open Source Software*. Berkeley, CA, USA: Apress, 2021, pp. 187–240.

[44] Association for the Advancement of Medical Instrumentation, *American National Standard ANSI/AAMI EC13: 2002: Cardiac Monitors, Heart Rate Meters, and Alarms*, Arlington, VA, USA: AAMI, 2002.